


Original Article

Open Access



Investigating lysosomal dysfunction in Fabry disease using induced pluripotent stem cell-derived podocytes

Caitlin R. Ryan¹, Andrea F. Wise¹, Elisha Tindoy¹, Shoni Bruell¹, Maria Fuller², Kathleen M. Nicholls³, Sharon D. Ricardo¹ 

¹Department of Pharmacology, Biomedicine Discovery Institute, Monash University, Clayton, Victoria 3800, Australia.

²Genetics and Molecular Pathology, South Australia Pathology at Women's and Children's Hospital and Adelaide Medical School and School of Biological Sciences, University of Adelaide, Adelaide, SA 5006, Australia.

³Department of Nephrology, The Royal Melbourne Hospital and Department of Medicine (RMH), University of Melbourne, Parkville 3000, Australia.

Correspondence to: Prof. Sharon D. Ricardo, Department of Pharmacology, Biomedicine Discovery Institute, Monash University, 9 Ancora Imparo Way, Clayton, Victoria 3800, Australia. E-mail: sharon.ricardo@monash.edu

How to cite this article: Ryan CR, Wise AF, Tindoy E, Bruell S, Fuller M, Nicholls KM, Ricardo SD. Investigating lysosomal dysfunction in Fabry disease using induced pluripotent stem cell-derived podocytes. *J Transl Genet Genom.* 2025;9:48-61. <https://dx.doi.org/10.20517/jtgg.2024.87>

Received: 25 Oct 2024 **First Decision:** 20 Jan 2025 **Revised:** 3 Feb 2025 **Accepted:** 12 Feb 2025 **Published:** 26 Feb 2025

Academic Editor: Sanjay Gupta **Copy Editor:** Fangling Lan **Production Editor:** Fangling Lan

Abstract

Aims: This study used induced pluripotent stem cell-derived podocytes from a Fabry disease (FD) patient carrying the p.Met284Thr pathogenic variant as an *in vitro* model to investigate lysosomal abnormalities driving cell pathology. Proteomic analysis was used to assess changes in lysosomal protein abundance in FD podocytes compared to controls. Additionally, temporal changes in lysosome number in FD podocytes were analyzed using automated live-cell imaging.

Methods: Label-free mass spectrometry proteomics was performed on FD podocytes at day 10 of differentiation compared to controls. For live-cell imaging, cultured podocytes were transfected with CellLight Lysosomes-GFP and Plasma Membrane-CFP, and then visualized and quantified on days 10 and 20 post-differentiation using a Perkin Elmer Phenix High Content Screening Microscope.

Results: Proteomic analysis showed dysregulation of glycosphingolipid metabolism proteins, including decreased galactosidase alpha (GLA; $P < 0.01$) and increased galactosylceramidase and glucosylceramidase ($P < 0.01$) in FD



© The Author(s) 2025. **Open Access** This article is licensed under a Creative Commons Attribution 4.0 International License (<https://creativecommons.org/licenses/by/4.0/>), which permits unrestricted use, sharing, adaptation, distribution and reproduction in any medium or format, for any purpose, even commercially, as long as you give appropriate credit to the original author(s) and the source, provide a link to the Creative Commons license, and indicate if changes were made.



podocytes. Lysosomal proteins were enriched, with a significant increase in cathepsin B ($P < 0.001$) and a decrease in lipase A ($P < 0.01$). Furthermore, the dysregulation of proteins involved in cell cycle regulation and growth signaling pathways, such as polo-like kinase 1 (PLK1; $P < 0.0001$) and proto-oncogene tyrosine-protein kinase Src (SRC; $P < 0.01$), suggested broader impacts on cellular processes. Temporal live-cell imaging revealed a significant increase in lysosome number in day 20 FD podocytes compared to day 10 FD podocytes and controls ($P < 0.01$).

Conclusions: These findings collectively suggest that FD podocytes undergo progressive lysosomal impairment, which may contribute to cellular dysfunction and disease progression. These proof-of-concept findings lay a foundation for future research on targeted FD therapies using high-throughput screening and advanced analytical techniques.

Keywords: Fabry disease, lysosomes, podocytes, induced pluripotent stem cells, proteomics, live-cell imaging

INTRODUCTION

Fabry disease (FD) is the most common X-linked lysosomal storage disorder and is caused by pathogenic variants in the *GLA* gene, leading to a deficiency in lysosomal α -galactosidase A (α -Gal A)^[1,2]. This enzyme deficiency results in the progressive accumulation of globotriaosylceramide (Gb3), especially in kidney podocytes, contributing to FD nephropathy, proteinuria, and chronic kidney disease (CKD). Although therapies such as enzyme replacement therapy (ERT) can reduce Gb3 levels, the reversal of kidney damage remains incomplete, particularly in podocytes, which exhibit slower and less complete Gb3 clearance compared to other renal cell types^[3-5].

Lysosomal dysfunction is a hallmark of FD, driven by Gb3 accumulation due to α -Gal A deficiency. Accumulation of globotriaosylsphingosine (lysoGb3), deacetylated Gb3, is thought to exacerbate these processes, driving fibrosis and inflammatory responses and further impairing lysosomal function in FD nephropathy^[6-8]. While it is well understood that this buildup disrupts normal lysosomal function and leads to podocyte injury, many aspects of the cellular consequences of lysosomal dysfunction remain unclear. Gb3 accumulation has been shown to impair autophagy^[9] and promote ferroptosis^[10], and increase podocyte stress, leading to cell depletion^[4,11-14], yet the precise signaling pathways that contribute to lysosomal dysfunction and progressive organ damage are not yet fully understood.

To better understand these mechanisms, induced pluripotent stem cell (iPSC)-derived podocytes offer a promising alternative to primary podocytes, which are difficult to maintain in culture. These iPSC-based models can replicate patient-specific genetic and phenotypic characteristics, offering a promising platform for understanding the molecular mechanisms underlying FD and for therapeutic screening, as we have previously reported in podocytes^[10] and cardiomyocytes^[15]. We now provide evidence of the proteomic and cellular changes occurring in FD podocytes, which collectively highlights the significant impact of lysosomal dysfunction on podocyte homeostasis. iPSCs were derived from FD patients and compared to controls, which were then differentiated into kidney podocytes as previously reported^[10,16-18].

This study represents the first to comprehensively characterize the proteomic and temporal changes in lysosomal dynamics in human iPSC-derived podocytes from an individual with FD carrying the p.Met284Thr *GLA* variant. Using advanced proteomic analysis and automated live-cell imaging, we provide insights into the lysosomal abnormalities that may drive disease progression in podocytes. This model offers a human-relevant system for investigating FD mechanisms, with implications for developing more targeted therapies aimed at ameliorating lysosomal dysfunction in FD nephropathy.

MATERIALS AND METHODS

Derivation and differentiation of iPSC-derived podocytes

iPSCs were derived from dermal fibroblasts collected via a punch biopsy from a male FD patient carrying the p.Met284Thr *GLA* variant and who presented with renal and cardiovascular disease, as previously described^[10]. Two age-matched control lines were also reprogrammed following informed consent. Podocyte differentiation followed Wise *et al.*'s protocol^[10,16], using DMEM/F12 with FBS, NEAA, penicillin-streptomycin, activin A, bone morphogenetic protein 7 (BMP7), retinoic acid, β -mercaptoethanol and Y-27632 (ROCK inhibitor) for enhanced attachment. Media changes occurred every other day for 10 days, with activin A, BMP7, and retinoic acid removed for long-term culture.

Transmission electron microscopy

Differentiated podocytes were isolated and fixed in Karnovsky's fixative and washed in 1 mL 0.1 M cacodylate buffer before post-fixation in 1% osmium tetroxide for one hour at room temperature. Serial dehydration was performed before embedding in resin. Pellets were thin-sectioned with an ultra-microtome and placed in copper orthogonal grids before staining with 4% uranyl acetate. All sections were imaged using a Hitachi H7500 transmission electron microscopy (TEM) (Hitachi) or Tecnai T12 TEM (FEI) with Gatan Microscopy Suite Software (Gatan Incorporated). Image J was used to quantify the percentage of lysosomal area per field and lysosome size in control and FD podocytes taken at $\times 10,000$ magnification.

Proteomic analysis and enrichment studies

Proteomic data were analyzed to identify key differences between FD and control iPSC-derived podocytes. Proteomic analysis was performed with liquid chromatography and tandem mass spectrometry (LC-MS/MS) on FD iPSC-derived podocytes or two pooled control lines using triplicate pellets via label-free quantification (LFQ) as previously detailed^[10]. Sample preparation involved solubilization in SDS buffer, sonication for DNA shearing, and clarification via centrifugation. Protein quantification was carried out using the BCA Protein Assay, followed by digestion with trypsin using S-Traps. Peptides were purified by solid-phase extraction and analyzed using a Dionex UltiMate 3000 system coupled to an Orbitrap Eclipse Tribrid mass spectrometer. Separation occurred on C18 columns under optimized acetonitrile gradients, with ionization performed via nanoelectrospray and FAIMS for gas-phase separation.

Data were acquired in a data-dependent mode, with high-resolution scans for both precursor ions and fragments, employing FAIMS compensation voltages. Processing of raw data was performed using Fragpipe, with protein quantification by LFQ match-between-runs (LFQ-MBR) and searches against the SwissProt human proteome. LFQ-Analyst was used for differential protein analysis, applying limma for statistical modeling, with cut-offs set at an adjusted *P*-value < 0.05 and \log_2 fold-change > 1 .

Proteomic data analysis and visualization

Principal component analysis (PCA) was conducted to visualize variance between samples. Hierarchical clustering for heatmap generation was performed using the ComplexHeatmap package in R, as previously reported^[10]. Differentially expressed proteins were selected based on a \log_2 fold change > 1 and an adjusted *P*-value < 0.05 . Enrichment analysis using gene ontology (GO) and Kyoto Encyclopedia of genes and genomes databases (KEGG) provided biological insights, with results visualized using bar and line charts for enriched pathways. GO enrichment analysis was conducted to identify overrepresented biological processes, molecular functions, and cellular components among differentially expressed proteins. Enriched terms were visualized as bubble plots, with bubble size indicating gene count and the X-axis indicating the level of statistical significance. A smaller $-\log_{10}$ (adjusted *P* value) indicates greater statistical significance (*P*-value < 0.05). Volcano plots were created using LFQ-Analyst to visualize differential protein abundance, plotting \log_2 fold change against the negative \log_{10} of the adjusted *P*-value. Proteins with significant up- or downregulation were highlighted. A full protocol, including details on peptide purification,

chromatography, and data processing parameters, has been previously published^[10].

Temporal visualization of cellular components using CellLight staining

To visualize lysosomes and cell components in cultured podocytes in real time, the cells were transfected with CellLight reagents, which express fluorescently tagged proteins targeted to specific organelles. On Day 8 of differentiation, cells were plated at 2,500 cells per well in black-walled 96-well plates coated with Geltrex (Gibco) and incubated for 24 h under optimal conditions (37 °C, 5%CO₂, and humidity). On Day 9, the cells were transfected with CellLight Lysosomes-green fluorescent protein (GFP; LAMP-1, Invitrogen) at 25 particles per cell, which emits green fluorescence (Excitation: 488 nm, Emission: 510 nm), and CellLight Plasma Membrane-cyan fluorescent protein (CFP, Invitrogen), which targets the plasma membrane via the myristoylation/palmitoylation sequence from Lck tyrosine kinase, transfected at 25 particles per cell (Excitation: 435 nm, Emission: 485 nm).

After a 16-h incubation period to allow for the expression of the fluorescently tagged proteins, on Day 10, the iPSC-podocytes were stained with 1 µM Hoechst 33342 to visualize the nuclei. Live-cell imaging was performed using the Perkin Elmer Opera Phenix High Content Screening Microscope in a 37 °C, 5%CO₂, humid environment to ensure cell viability during imaging. Cells were re-transfected on Day 19 with CellLight Lysosomes-GFP at 10 particles per cell, CellLight Plasma Membrane-CFP at 10 particles per cell, and CellLight Late Endosomes-red fluorescent protein (RFP, Invitrogen), which targets Rab-7a and emits red fluorescence (Excitation: 555 nm, Emission: 584 nm), at 25 particles per cell. This enabled continued monitoring of lysosome/organelle dynamics over the time of podocyte differentiation. In addition, podocytes were incubated with 50 nM LysoTracker Red (Invitrogen), diluted in pre-warmed podocyte differentiation medium (without additional supplements) for 30 min to allow for lysosome-specific staining, or immunofluorescence staining with a mouse monoclonal LAMP-2 antibody (Abcam, clone H4B4). Podocytes were imaged 20 days post differentiation using the Perkin Elmer Phenix High Content Screening Microscope under optimal incubation conditions.

Analysis of LAMP-1+ lysosomal accumulation

The built-in Harmony software of the Perkin Elmer Opera Phenix High Content Screening Microscope enabled real-time quantitative analysis of the fluorescence intensity of CellLight and LysoTracker-stained lysosomes. Key metrics such as the number of LAMP-1+ vesicles and cellular area were recorded over time of culture in FD podocytes and controls. Baseline manual adjustments were made to the image analysis parameters, such as threshold settings for fluorescence intensity, to exclude background noise and focus on lysosome-specific signals within the cellular boundaries. Artifacts or any non-specific fluorescence were excluded through stringent gating parameters to ensure high specificity and consistency of the analysis across comparisons. In addition to quantifying lysosomes, their spatial distribution within the cell cytosol was examined. This provided a more comprehensive understanding of lysosomal dynamics in iPSC-podocytes during their differentiation into mature podocytes over the 20 days of differentiation.

Statistical analysis

The data collected from the image analysis were exported from the Harmony software v5.1.2167.302 and processed for further statistical evaluation, with outputs per cell including lysosome number, area, and intensity. Data were analyzed using GraphPad Prism v10.0.02, with results presented as mean ± SEM. The non-parametric Kruskal-Wallis test was used for comparing groups, with Dunn's post-hoc test applied for multiple comparisons. Statistical significance was defined as $P < 0.05$.

RESULTS

Lysosomal morphology in FD podocytes

TEM analysis revealed distinct morphological differences in lysosomes between control and FD podocytes at day 10 of differentiation. Control podocytes displayed well-formed, rounded lysosomes that appeared small and electron-dense, uniformly distributed within the cytoplasm [Figure 1A]. In contrast, FD podocytes exhibited markedly enlarged and irregularly shaped lysosomes, presenting as electron-dense deposits [Figure 1B] or enlarged myelin bodies [Figure 1C], both characteristic of FD. These lysosomal inclusions were suggestive of the accumulation of undigested substrates, consistent with the pathological features observed in FD.

Quantitative analysis of the lysosomal area demonstrated a significant increase in lysosomal area in FD podocytes compared to controls [Figure 1D and E]. These findings highlight lysosomal enlargement and morphological abnormalities present in FD podocytes, correlating with the known dysfunction of α -Gal A activity and Gb3 substrate accumulation characteristic of the disease.

Proteomic analysis shows clear differences between FD and control podocytes

iPSC-derived podocytes from a FD patient carrying the p.Met284Thr *GLA* variant were previously confirmed to have a significant reduction in α -Gal A activity and increased Gb3 accumulation compared to control podocytes^[10]. In Figure 2A, Principal Component Analysis (PCA) was used to dimensionally condense the large proteomic data set by reducing it to linear principal components that capture the differences between FD and control podocytes. PC1 represents 29.4% of variance along the X-axis, while PC2 represents 11.2% of variance along the Y-axis. The results showed that FD podocytes grouped distinctly from controls, highlighting major differences in their protein profiles.

Hierarchical clustering in the heatmap [Figure 2B] showed distinct patterns of protein abundance, represented by clear clusters of proteins that were either higher or lower in FD podocytes compared to controls. This highlights specific molecular changes, including pathways involved in lysosomal function and cellular organization. Figure 2C provides a Venn diagram that shows the overlap and distinct proteomic profiles between control and FD podocytes. A total of 5,971 proteins (89%) were shared between the control and FD podocytes, indicating a significant overlap. However, 581 proteins (9%) were uniquely identified in control podocytes, with 188 proteins (3%) unique to FD podocytes. This indicates that although there is a considerable shared proteomic baseline, FD podocytes exhibit a distinct subset of proteins, highlighting the specific molecular alterations associated with the pathogenic *GLA* variant and the resulting lysosomal dysfunction.

Further analysis of key enzymes involved in glycosphingolipid metabolism provided deeper insights into the specific pathways disrupted in FD podocytes. Box plots for *GLA*, glucosylceramidase (*GBA*), and galactosylceramidase (*GALC*) proteins [Figure 2D] showed significant alterations in their expression levels in FD podocytes compared to controls. *GLA* (encoding α -Gal A) was expectedly reduced in FD podocytes, while *GBA* and *GALC*, both enzymes involved in glycosphingolipid degradation, displayed compensatory upregulation. These data suggest potential cellular responses to the accumulation of Gb3 and other substrates in FD podocytes. A summary of the glycosylceramide catabolic process is represented in Figure 2E, indicating how protein abundance shifts observed in FD podocytes align with known metabolic disruptions. The decreased activity of α -Gal A leads to Gb3 accumulation, while compensatory upregulation of *GBA* and *GALC* suggests an attempt to process excess glycolipids through alternate degradation pathways.

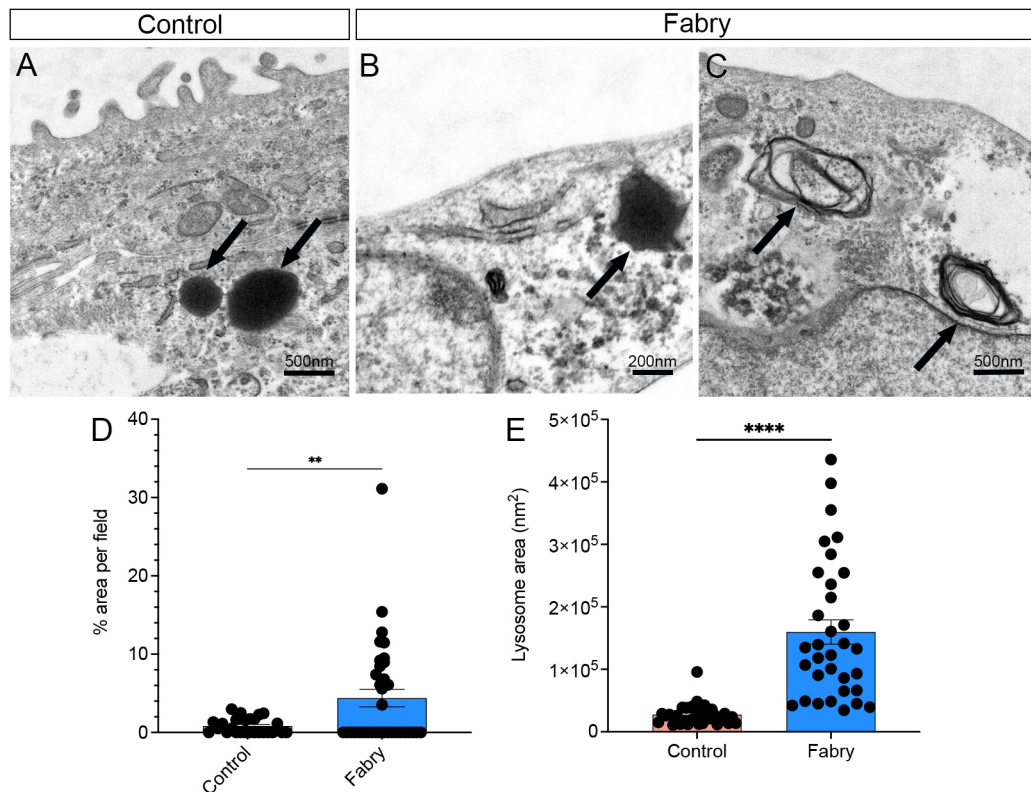


Figure 1. Lysosomal morphology and quantification in FD iPSC-podocytes. (A) Transmission Electron Microscopy (TEM) image of control iPSC-podocytes at day 10 of differentiation, showing rounded and electron-dense lysosomes in the cytosol (indicated by arrows). (B) TEM image of FD podocytes, showing enlarged and irregularly shaped lysosomes (arrows) and (C) myelin bodies (arrows), characteristic of FD. (D) FD podocytes show a significantly greater lysosomal area per field compared to controls on day 10 (** $P < 0.01$), which (E) correlated with a significant total lysosomal area (**** $P < 0.0001$). Representative quantitative analysis of lysosomal area in FD and control podocytes, providing further validation of lysosomal dysregulation in FD. Data are presented as mean \pm SEM.

Gene ontology and proteomic pathway enrichment analysis

To further investigate the proteomic alterations in FD podocytes, GO enrichment analysis was performed to identify over-represented biological processes, molecular functions, and cellular components associated with the differentially expressed proteins. Figure 3A displays the top enriched pathways, highlighting key terms such as lysosome, intracellular organelle lumen, lysosomal lumen, and glycosylceramide catabolic process, which are consistent with the known disruptions in lysosomal storage and lipid metabolism in FD. A volcano plot of the differentially expressed proteins is shown in Figure 3B, highlighting proteins that are significantly upregulated (blue) or downregulated (red) in FD podocytes compared to controls. Notably, several lysosomal and metabolic proteins were found to be significantly altered in FD podocytes, consistent with the known lysosomal dysfunction in FD. The most altered proteins included the downregulation of polo-like kinase 1 (PLK1), involved in cell cycle regulation, and the upregulation of the proto-oncogene tyrosine-protein kinase Src (SRC), which plays a role in signaling pathways regulating cell growth and differentiation.

The pathway enrichment findings were visually summarized in a cellular component map shown in Figure 3C, which illustrates key proteins localized to the lysosome and involved in lipid degradation, including GLA, GBA, and GALC, all of which are essential components of the glycosphingolipid degradation pathway. Additionally, proteins involved in proteoglycan metabolism and extracellular matrix

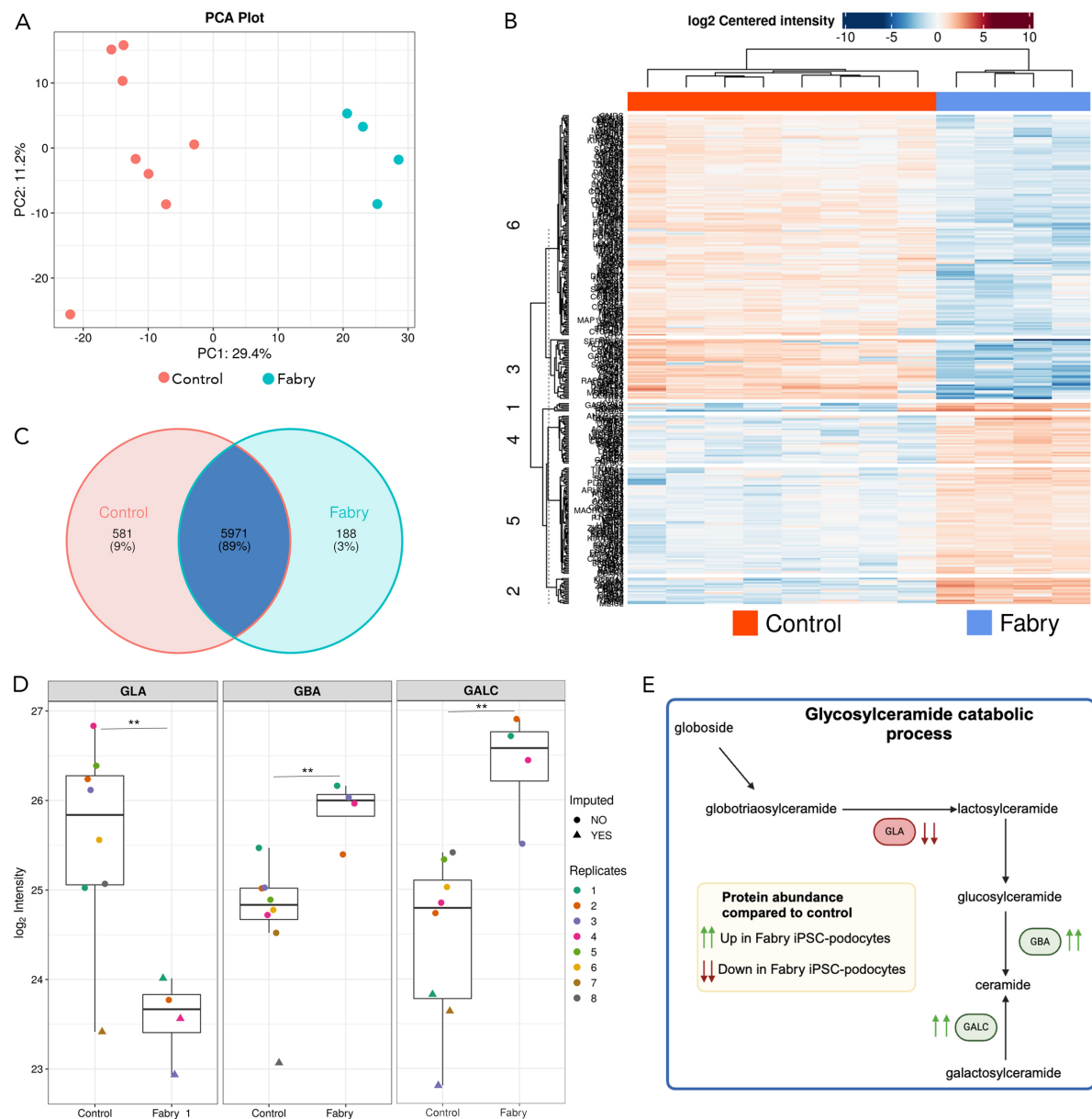


Figure 2. Differential protein abundance and functional pathways in FD and control iPSC-podocytes. (A) Principal component analysis (PCA) plot illustrating the variance in protein abundance between FD (blue) and control (red) podocytes. (B) Heatmap of differentially expressed proteins in FD and control iPSC-podocytes, showing distinct clustering. (C) Venn diagram depicting the overlap of proteins identified in FD and control podocytes. The majority of proteins (5971) were shared between both groups, while differentially abundant proteins were observed in control (9%) and FD (3%) podocytes. (D) Box plots illustrating the relative abundance of key enzymes involved in glycosylceramide metabolism: GLA, GALC, and GBA in FD podocytes compared to controls. (E) Schematic representation of the glycosylceramide catabolic pathway, highlighting the altered abundance of proteins in FD podocytes. Proteins upregulated in FD podocytes are indicated with green upward arrows, while proteins downregulated are indicated with red downward arrows. $n = 4$ replicates per iPSC-podocyte line. $^{**}P < 0.01$ using student's t -test. GALC: Galactosylceramidase; GBA: glucosylceramidase beta; GLA: galactosidase alpha.

organization were identified, including lumican (LUM), collagen type VI alpha-1 (COL6A1), and glypican 4 (GPC4). These findings suggest that FD podocytes exhibit alterations not only in lysosomal function but also in the extracellular matrix and cell-matrix interactions, potentially contributing to the kidney

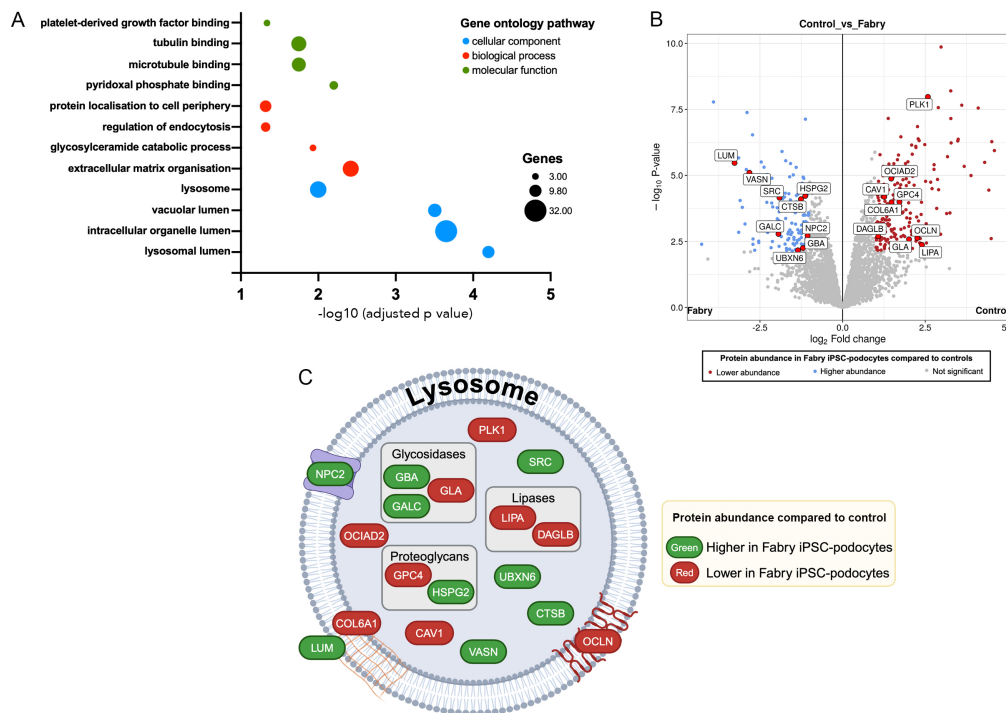


Figure 3. Dysregulation of lysosomal proteins in FD podocytes. (A) Gene ontology (GO) term enrichment analysis of FD podocytes, highlighting significantly enriched pathways related to cellular components, biological processes, and molecular functions. Several genes were involved in these pathways, indicated by the increasing size of the colored circles and significantly enriched proteins were identified based on a false discovery rate < 0.05 . (B) Volcano plot showing differential protein abundance in FD podocytes relative to controls, with upregulated proteins in FD podocytes (blue) and downregulated proteins (red) highlighted. (C) A schematic representation of the lysosome showing specific proteins that are upregulated (green) and downregulated (red) in FD podocytes relative to controls. $n = 4$ replicates per iPSC-podocyte line. CAV1: Caveolin 1; COL6A1: collagen type IV alpha 1 chain; CTSB: cathepsin B; DAGLB: diacylglycerol lipase beta; GALC: galactosylceramidase; GBA: glucosylceramidase; GLA: galactosidase alpha; GO: Gene Ontology; GPC4: glypican 4; HSPG2: heparan sulfate proteoglycan 2; LIPA: lipase A; LUM: lumican; NPC2: Niemann-Pick disease type C2 protein; OCIAD2: OCIA domain-containing protein 2; OCLN: occludin; PLK1: polo-like kinase 1; SRC: proto-oncogene tyrosine-protein kinase; UBXN6: UB domain-containing protein 6; VASN: vasorin.

dysfunction observed in FD patients. Together, these results emphasize the disruption of lysosomal and glycolipid degradation pathways in FD podocytes, alongside changes in the cytoskeleton, cell signaling, and extracellular matrix organization, contributing to the unique pathological phenotype of FD.

Lysosome and endosome visualization in FD podocytes

To confirm the lysosomal specificity of markers in FD podocytes, we performed LAMP-1-GFP transfection and co-stained the cells with various markers of lysosomal and endosomal compartments over 20 days of differentiation. [Figure 4](#) provides representative images highlighting the successful transfection of FD podocytes with LAMP-1-GFP, a well-established lysosomal membrane protein marker. In [Figure 4A](#), the colocalization of LAMP-1-GFP with LysoTracker demonstrates that the GFP-tagged LAMP-1 specifically targets lysosomal compartments. [Figure 4B](#) further confirms the specificity of LAMP-1-GFP by colocalizing with Rab7a-RFP, a marker for late endosomes, with a merged image highlighting the connectivity between lysosomal and late endosomal compartments. Additionally, immunofluorescence staining for LAMP-2 [[Figure 4C](#)], another lysosomal membrane-associated protein, was performed, although cell colocalization was not viable due to the requirement for fixation post transfection.

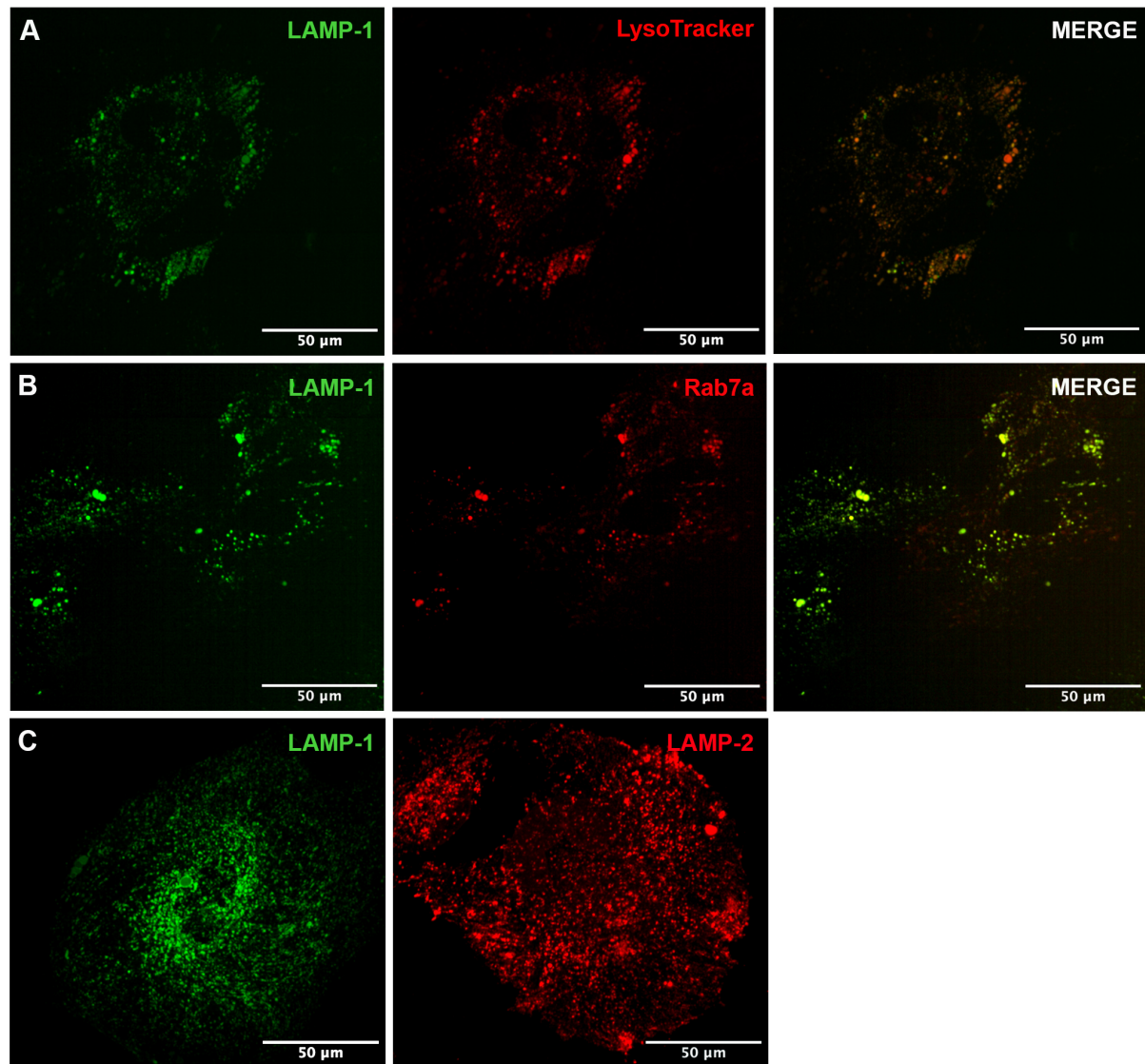


Figure 4. Specificity of LAMP-1-GFP transfection in FD podocytes. (A) Visualization of LAMP-1-GFP transfection alongside LysoTracker Red staining in FD podocytes after 20 days of differentiation, showing colocalization in lysosomal compartments. (B) Colocalization of LAMP-1-GFP and Rab7a-RFP transfection constructs in FD podocytes, highlighting lysosomal and late endosomal compartments. (C) Representative images showing LAMP-1-GFP transfection alongside immunofluorescence staining for LAMP-2 FD podocytes. Note that the images in (C) represent two different cells; hence, no colocalization was possible. Scale bars represent 50 µm. GFP: Green fluorescent protein; LAMP-1: lysosome-associated membrane protein-1; LAMP-2: lysosome-associated membrane protein-2; RFP: red fluorescent protein.

LAMP-1+ lysosomal accumulation in FD podocytes

Phase contrast imaging [Figure 5A] provided an overview of podocyte morphology, serving as a foundational reference for subsequent live-cell imaging experiments. Temporal lysosomal accumulation was assessed using live-cell imaging in FD podocytes compared to control cells following LAMP-1-GFP transfection in reference to plasma membrane-CFP transfection and Hoechst cell nuclear staining [Figure 5B and C]. Real-time automated image analysis was conducted using Harmony software, enabling the detailed capture of cellular features such as the nucleus [Figure 5D], cytoplasm [Figure 5E], and LAMP-1+ lysosomes [Figure 5F]. This automated analysis allowed for the high-throughput identification

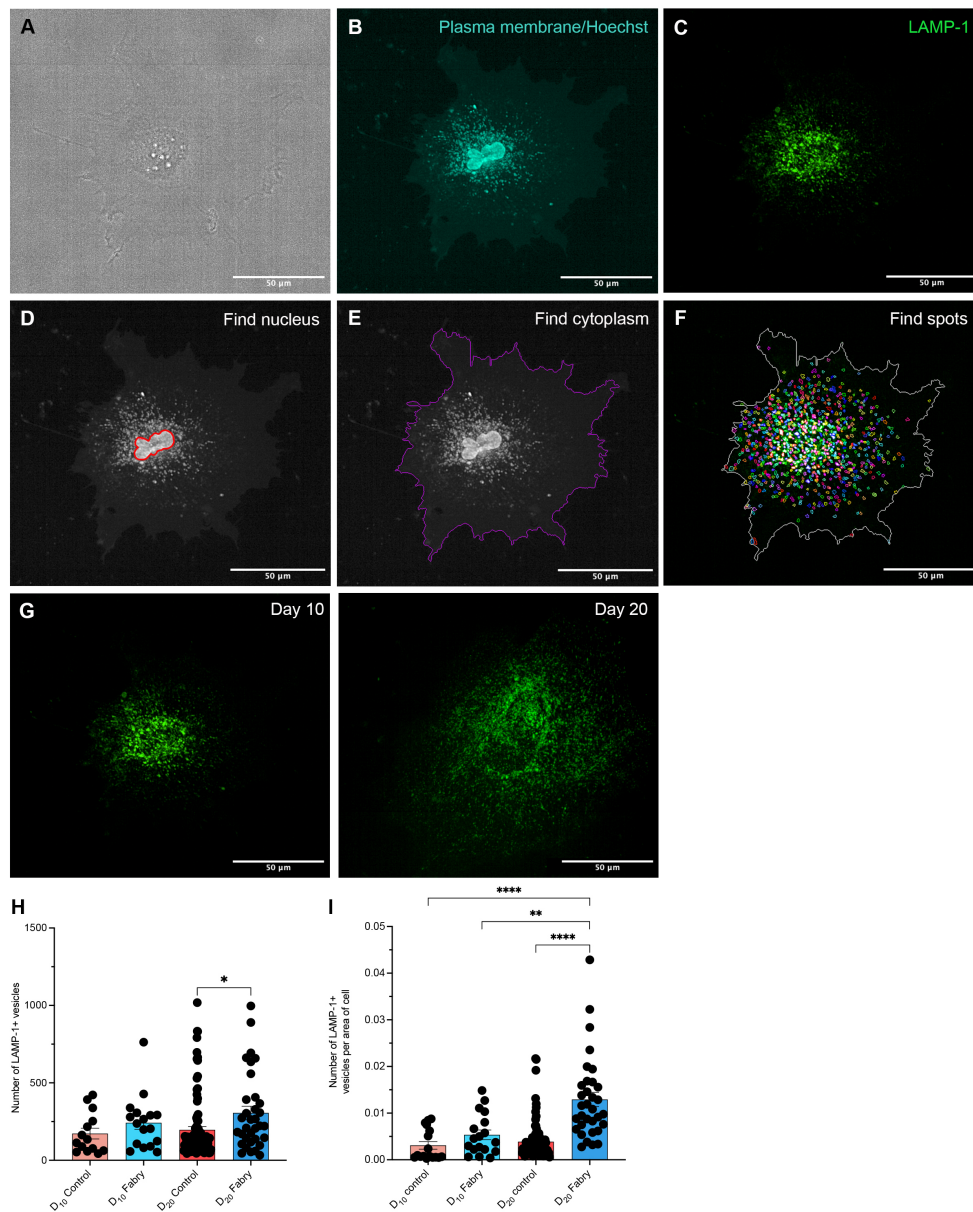


Figure 5. LAMP-1+ lysosomal accumulation in FD podocytes visualized through automated image analysis. (A) Representative images of a FD podocyte after 10 days of differentiation under brightfield, (B) CFP, and (C) GFP channels, showing plasma membrane, nucleus, and LAMP-1+ lysosomes. (D-F) Real-time automated cellular analysis using Harmony software to identify the: (D) nucleus, (E) cytoplasm, and (F) number and area of LAMP-1+ vesicles (termed spots) in FD podocytes. (G) Real-time localization of LAMP-1+ lysosomes in FD podocytes over time of differentiation on days 10 and 20. (H) Quantification of the mean number of LAMP-1+ lysosomes per cell; and (I) LAMP-1+ lysosome number as a proportion of total cell area in FD versus control podocytes at day 10 and day 20 time points. Scale bars represent 50 μ m. Data are presented as mean \pm SEM. Statistical significance is indicated as * P < 0.05, ** P < 0.01, **** P < 0.0001, using the Kruskal-Wallis test with Dunn's post-hoc test. CFP: Cyan fluorescent protein; GFP: green fluorescent protein; LAMP-1: lysosome-associated membrane protein-1.

and unbiased quantification of cellular properties, using Hoechst staining to detect nuclei and CFP-transfected cytoplasm correlated with GFP-transfected LAMP-1+ vesicles, capturing the same cells in real time.

On day 10, FD podocytes displayed fewer LAMP-1+ lysosomes compared to day 20 FD podocytes, with a significant increase in lysosomal accumulation that was evident over time [Figure 5G]. Quantification of lysosomal number per cell [Figure 5H] showed a significant increase in FD podocytes at day 20 compared to controls ($P < 0.05$), indicating progressive lysosomal changes following the differentiation period. Using the plasma membrane-CFP transfection construct [Figure 5E], cellular area was quantified in conjunction with the number of LAMP-1+ lysosomes [Figure 5F]. When normalized to the total cellular area, significant increases in the number of LAMP-1+ vesicles were observed in day 20 FD podocytes compared to both day 10 and day 20 control podocytes (Figure 5I; $P < 0.0001$). A significant increase in LAMP-1+ vesicles as a proportion of cellular area was also observed in day 20 FD podocytes compared to day 10 FD podocytes (Figure 5I; $P < 0.01$).

DISCUSSION

Our study combines proteomics and advanced live-cell imaging to assess lysosomal dysfunction in FD using patient-derived iPSC-podocytes. Proteomic analysis identified a significant dysregulation of lysosomal proteins involved in the glycosphingolipid pathway, which aligns with the established dysfunction of lysosomal Gb3 storage in FD progression. Automated live-cell imaging revealed a time-dependent increase in LAMP-1+ lysosomes in FD podocytes, demonstrating a progressive accumulation in lysosomal number. When normalized to cell area, there was a significant increase in lysosomal number in day 20 cultured FD podocytes compared to day 10 podocytes and controls, indicating persistent lysosomal stress and cellular dysfunction.

Elevated plasma Gb3 and lysoGb3 are well-established hallmarks of FD^[6-8], and although lysosomal Gb3 storage is a key factor in disease manifestation, the formation of pathogenic lysoGb3 likely plays a significant role in the onset and progression of symptoms^[19,20]. In our study, proteomic analysis identified significant dysregulation of proteins involved in lysosomal storage and lipid degradation, supporting previous studies that link Gb3 accumulation to disrupted lysosomal function, leading to cellular damage and multi-organ pathology^[5,15,21]. This accumulation has been linked to reactive oxygen species production and mitochondrial impairment in podocytes, further damaging the tubular epithelium^[21] and leading to subsequent podocyte damage, which extends to the tubular epithelium^[19]. Although inhibiting Notch1 shows promise in mitigating these effects^[22], current treatments, including ERT, do not fully reverse the underlying pathology^[4,5,23]. Even after prolonged ERT treatment, the reversal of lysosomal dysfunction in podocytes remains insufficient, as shown in the persistence of structural damage and with new therapeutic targets, such as α -synuclein (SNCA)^[5]. Delaleu *et al.* demonstrated that early ERT only partially reverts gene expression patterns associated with FD nephropathy, indicating that significant pathways, including those related to transporter activity, remain dysregulated or re-emerge despite treatment^[4].

The differentiation of podocytes from patient-derived iPSCs offers direct insights into the disease mechanisms within affected cells, complementing proteomic studies using FD patient plasma that have highlighted inflammatory and angiogenesis-related proteins^[13,14,24]. In this study, we observed a significant dysregulation of lysosomal proteins, consistent with previous research in cardiomyocytes and podocytes, which are the most affected cell types in FD^[1,12,25]. The downregulation of the main effector protein, GLA, aligns with the expected disease phenotype^[5,15,26]. In contrast, the upregulation of enzymes such as GBA and GALC suggests a *de novo* compensatory response to manage lipid accumulation, as evidenced by clinical trials showing substrate reduction therapy (SRT) efficacy in reducing Gb3 and lysoGb3 levels^[27,28]. These findings collectively demonstrate that FD podocytes exhibit widespread proteomic alterations, particularly in pathways related to lysosomal function and glycolipid metabolism, which may contribute to disease pathology and the cellular phenotype observed in FD nephropathy.

Beyond the glycosphingolipid pathway, we identified significant dysregulation of other lysosomal proteins, including cathepsin B, lipase A (LIPA), and COL6A1. The upregulation of cathepsin B suggests enhanced lysosomal protease activity, possibly as a response to accumulated substrates. Conversely, the downregulation of LIPA and COL6A1 indicates disruptions in lipid degradation and lysosomal structural integrity. Additionally, lysosomal membrane proteins such as LUM and Niemann-Pick disease type C2 protein (NPC2) were upregulated, suggesting compensatory cellular remodeling due to lysosomal dysfunction. The reduced abundance of structural proteins like COL6A1 and occludin (OCLN) suggests disruptions in lysosomal and broader cellular architecture, consistent with previous reports^[5,26]. This study provides evidence for the involvement of lysosomal proteins beyond glycosphingolipid metabolism in FD pathology. The integration of proteomic analysis with automated live-cell imaging offers a robust platform for further exploration of disease-specific cellular mechanisms.

The advanced image analysis used in this study is the first to quantitatively visualize lysosome accumulation in FD podocytes in real time, allowing us to capture dynamic changes in lysosomal numbers, size, and distribution with disease progression over time of culture. This live cell imaging approach enabled a more accurate assessment of lysosomal stress and dysfunction compared to traditional static methods, offering a deeper understanding of the pathological mechanisms driving FD nephropathy. Using an unbiased, automated quantification of LAMP-1+ lysosomes in FD podocytes, we observed a significant increase in the size and number of LAMP-1+ vesicles compared to controls, reflecting heightened lysosomal stress. This technique allowed us to track changes in real time, offering a more comprehensive understanding of how lysosomal dysfunction evolves during podocyte differentiation due to a FD pathogenic variant. The persistence of lysosomal stress in FD podocytes over later stages of differentiation suggests that these podocytes continue to undergo significant dysfunction, which could contribute to ongoing podocyte injury and the progression of FD nephropathy.

This study provides valuable insights into lysosomal dysfunction in FD podocytes; however, several limitations must be acknowledged. First, the investigation focuses on a single case utilizing iPSC-derived podocytes from a patient with the p.Met284Thr pathogenic variant. Future studies should include larger cohorts of male and female patients with different *GLA* mutations to validate these findings and assess variability across genetic and demographic subgroups. Second, lysosomal alterations are known to occur in various cell types, and the extent to which the observed changes are specific to podocytes remains unclear. Further research is required to determine whether similar lysosomal impairments and downstream cellular disruptions occur in other affected renal cell types, such as mesangial or epithelial cells, and whether the clinical manifestations arise from cell-specific genetic profiles or shared systemic mechanisms. Finally, while the proteomic and imaging approaches employed here provide robust *in vitro* insights into lysosomal dysfunction and its progression, translating these findings to *in vivo* systems and clinical settings is necessary to fully understand their implications for disease progression and therapeutic development.

In conclusion, our study highlights the utility of iPSC-derived podocytes as a model for FD, combining quantitative proteomics and advanced imaging to offer insights into disease pathology. The progressive increase in lysosomal size and number reflects ongoing dysfunction, underscoring the need for therapeutic strategies targeting lysosomal functional clearance of Gb3. The culture of iPSC-derived podocytes may not only facilitate the identification of novel therapeutic targets but also support high-throughput screening of potential therapies, aiming to reverse lysosomal dysfunction and improve clinical outcomes for FD patients.

DECLARATIONS

Acknowledgments

The authors would like to express their gratitude for the technical expertise and facilities provided by the Monash Biomedicine Discovery Institute Organoid Program. Special thanks to Monash MicroImaging, the Monash Proteomics and Metabolomics Facility, and the Monash Ramaciotti Centre for Cryo-Electron Microscopy at Monash University, Clayton Campus, for their invaluable support, expertise, and technical assistance. The authors also sincerely thank the patients and their families who contributed to this study by providing tissue samples.

Authors' contributions

Experiments: Ryan CR, Wise AF, Bruell S

Conceptual design: Wise AF, Fuller M, Nicholls KM, Ricardo SD

Wrote the manuscript: Ryan CR, Ricardo SD

Read and edited the manuscript: Ryan CR, Wise AF, Tindoy E, Bruell S, Fuller M, Nicholls KM, Ricardo SD

Availability of data and materials

The data discussed in this publication are accessible through <https://www.ebi.ac.uk/pride/>. Proteomics raw data are available via ProteomeXchange with the identifier PXD050848. iPSCs generated in this study will be available upon reasonable request; however, a completed Materials Transfer Agreement may be required.

Financial support and sponsorship

This study was supported by a philanthropic grant from the Honig family/Honig Medical Research Fellowship and funding from Shire/Takeda, Sanofi/Genzyme, and the Royal Melbourne Hospital Fabry Research Fund.

Conflicts of interest

Nicholls KM received research grant support and speaker/advisory board honoraria from Shire/Takeda, Sanofi/Genzyme, while the other authors have declared that they have no conflicts of interest.

Ethical approval and consent to participate

The research was carried out in accordance with the Declaration of Helsinki (2008) of the World Medical Association. Ethical approval was obtained from the Royal Melbourne Hospital Human Research Ethics Committee (66294/MH-2020) and Monash University Human Research Ethics Committee (Project number CF16/1247 – 2016000663). Informed consent was obtained from all participants.

Consent for publication

Not applicable.

Copyright

© The Author(s) 2025.

REFERENCES

1. Bokhari SRA, Zulfiqar H, Hariz A. Fabry Disease. Treasure Island, FL: StatPearls Publishing; 2025. [PubMed](#)
2. Chin SJ, Fuller M. Prevalence of lysosomal storage disorders in Australia from 2009 to 2020. *Lancet Reg Health West Pac.* 2022;19:100344. [DOI](#) [PubMed](#) [PMC](#)
3. Thurberg BL, Rennke H, Colvin RB, et al. Globotriaosylceramide accumulation in the Fabry kidney is cleared from multiple cell types after enzyme replacement therapy. *Kidney Int.* 2002;62:1933-46. [DOI](#)
4. Delaleu N, Marti HP, Strauss P, et al. Systems analyses of the Fabry kidney transcriptome and its response to enzyme replacement therapy identified and cross-validated enzyme replacement therapy-resistant targets amenable to drug repurposing. *Kidney Int.* 2023;104:803-19. [DOI](#)

5. Braun F, Abed A, Sellung D, et al. Accumulation of α -synuclein mediates podocyte injury in Fabry nephropathy. *J Clin Invest.* 2023;133:e157782. DOI
6. Talbot A, Nicholls K, Fletcher JM, Fuller M. A simple method for quantification of plasma globotriaosylsphingosine: utility for Fabry disease. *Mol Genet Metab.* 2017;122:121-5. DOI
7. Santostefano M, Cappuccilli M, Gibertoni D, et al. Fabry disease nephropathy: histological changes with nonclassical mutations and genetic variants of unknown significance. *Am J Kidney Dis.* 2023;82:581-96.e0. DOI
8. Maruyama H, Miyata K, Mikame M, et al. Effectiveness of plasma lyso-Gb₃ as a biomarker for selecting high-risk patients with Fabry disease from multispecialty clinics for genetic analysis. *Genet Med.* 2019;21:44-52. DOI PubMed PMC
9. Liebau MC, Braun F, Höpker K, et al. Dysregulated autophagy contributes to podocyte damage in Fabry's disease. *PLoS One.* 2013;8:e63506. DOI PubMed PMC
10. Wise AF, Krisnadevi IA, Bruell S, et al. Fabry disease podocytes reveal ferroptosis as a potential regulator of cell pathology. *Kidney Int Rep.* 2025;10:535-48. DOI PMC
11. Kim SY, Park S, Lee SW, et al. RIPK3 contributes to Lyso-Gb₃-induced podocyte death. *Cells.* 2021;10:245. DOI
12. Najafian B, Tøndel C, Svarstad E, Gubler MC, Oliveira JP, Mauer M. Accumulation of globotriaosylceramide in podocytes in Fabry nephropathy is associated with progressive podocyte loss. *J Am Soc Nephrol.* 2020;31:865-75. DOI PubMed PMC
13. Tebani A, Barbey F, Dormond O, et al. Deep next-generation proteomics and network analysis reveal systemic and tissue-specific patterns in Fabry disease. *Transl Res.* 2023;258:47-59. DOI
14. Tebani A, Mauhin W, Abily-Donval L, et al. A proteomics-based analysis reveals predictive biological patterns in Fabry disease. *J Clin Med.* 2020;9:1325. DOI
15. Ter Huurne M, Parker BL, Liu NQ, et al. GLA-modified RNA treatment lowers GB3 levels in iPSC-derived cardiomyocytes from Fabry-affected individuals. *Am J Hum Genet.* 2023;110:1600-5. DOI
16. Wise AF, Saini S, Ricardo SD. The differentiation of human induced pluripotent stem cells into podocytes in vitro. *Methods Mol Biol.* 2022;2454:317-25. DOI PubMed
17. Song B, Smink AM, Jones CV, et al. The directed differentiation of human iPS cells into kidney podocytes. *PLoS One.* 2012;7:e46453. DOI PubMed PMC
18. Lau RWK, Fisher C, Phan TK, et al. Modelling X-linked alport syndrome with induced pluripotent stem cell-derived podocytes. *Kidney Int Rep.* 2021;6:2912-7. DOI PubMed PMC
19. Aerts JM, Groener JE, Kuiper S, et al. Elevated globotriaosylsphingosine is a hallmark of Fabry disease. *Proc Natl Acad Sci USA.* 2008;105:2812-7. DOI PubMed PMC
20. Taguchi A, Ishii S, Mikame M, Maruyama H. Distinctive accumulation of globotriaosylceramide and globotriaosylsphingosine in a mouse model of classic Fabry disease. *Mol Genet Metab Rep.* 2023;34:100952. DOI PubMed PMC
21. Elsaid HOA, Rivedal M, Skandalou E, et al. Proteomic analysis unveils Gb₃-independent alterations and mitochondrial dysfunction in a gla^{-/-} zebrafish model of Fabry disease. *J Transl Med.* 2023;21:591. DOI PubMed PMC
22. Sanchez-Niño MD, Carpio D, Sanz AB, Ruiz-Ortega M, Mezzano S, Ortiz A. Lyso-Gb₃ activates Notch1 in human podocytes. *Hum Mol Genet.* 2015;24:5720-32. DOI
23. Beck M, Ramaswami U, Hernberg-Ståhl E, et al. Twenty years of the Fabry outcome survey (FOS): insights, achievements, and lessons learned from a global patient registry. *Orphanet J Rare Dis.* 2022;17:238. DOI PubMed PMC
24. Moore DF, Krokhin OV, Beavis RC, et al. Proteomics of specific treatment-related alterations in Fabry disease: a strategy to identify biological abnormalities. *Proc Natl Acad Sci USA.* 2007;104:2873-8. DOI
25. Chimenti C, Hamdani N, Boontje NM, et al. Myofilament degradation and dysfunction of human cardiomyocytes in Fabry disease. *Am J Pathol.* 2008;172:1482-90. DOI
26. Birket MJ, Raibaud S, Lettieri M, et al. A human stem cell model of Fabry disease implicates LIMP-2 accumulation in cardiomyocyte pathology. *Stem Cell Rep.* 2019;13:380-93. DOI PubMed PMC
27. Deegan PB, Goker-Alpan O, Geberhiwot T, et al. Venglustat, an orally administered glucosylceramide synthase inhibitor: assessment over 3 years in adult males with classic Fabry disease in an open-label phase 2 study and its extension study. *Mol Genet Metab.* 2023;138:106963. DOI PubMed PMC
28. Guérard N, Oder D, Nordbeck P, et al. Lucerastat, an iminosugar for substrate reduction therapy: tolerability, pharmacodynamics, and pharmacokinetics in patients with Fabry disease on enzyme replacement. *Clin Pharmacol Ther.* 2018;103:703-11. DOI